3-D Analysis of sinter processes by X-ray computer tomography

M. Nöthe*, K. Pischang*, P. Ponizil**, R. Bernhardt*, B. Kieback***

*Technische Universität Dresden
** Tomas Bata University, Zlin (Czech Republic)
*** Fraunhofer Institut für Angewandte Materialforschung, Dresden

Abstract

Microfocus computer tomography (µ-CT) gives the opportunity to observe the positions of individual particles in 3-D powder samples. The description of sinter processes, leading to the formation of bonds, the growth of sintering necks and particle centre approach, is based on two particle models. These models neglect the complex geometry of real powder specimens, like particle size distribution, irregular particle shape and inhomogeneous specimen densities. 2D models can be used to prove rearrangements of particles during sintering. These movements are attributed to the attempt to form low energy grain boundaries, asymetric sintering necks and stress caused by the inhomogenous particle centre approach. Up to now, an observation of particle movements inside of 3-D specimens has not been possible.
The first method to measure the particle arrangement in 3-D specimens is the µ-CT. In this paper the motions of spherical copper powder particles (average particle size 500…750 µm) during sintering are investigated. The positions of all particle centres were measured during several sintering stages. The analysis of movements with respect to the initial particle positions was performed by mathematical models. It is possible to prove movements of particles into larger pores, an increase of the average coordination number and the breaking of sintering necks.

Introduction

The optimisation of sinter processes requires detailed knowledge of the development of bonds between the individual particles and of the changes of particle constitution as well. Actually sinter models are based on the description of two particle boundaries and neglect the influence of particle constitution and often assume ideal contact zones between the particles [1,2]. Thus in the past great effort has been made to achieve experimental data, that are suitable to give a self-contained description of the complex geometries of real sinter specimens. Up to now this experiments were limited to the observation of rows of metal balls, 2D models and the observation of surfaces of 3-D models [3-6]. It is possible to follow translations and rotations of particles during sintering. The significant inconsistance between a theoretical description of shrinkage and the behaviour of real powder specimens during sintering is attributed to motions of whole particles. This movements occur due to the attempt to form low energy grain boundaries and stress caused by inhomogenous particle approach. Unfortunately the movements cannot be quantified on basis of the currently available experimental data. Microfocus computer tomography (µ-CT) is the first method to measure the particle arrangements inside of 3-D powder samples, giving the opportunity to analyse the particle motions in detail. The presented paper describes first experiments in process research using this method to create sequences of 3-D datasets describing several sintering stages of one sample.
Crucibles filled with copper powder were sintered in a hydrogen atmosphere. The sintering was interrupted several times to measure the particle distribution by µ-CT. The obtained data sets representing sequences of sintering stages were analysed by mathematical models. This

investigation allows the description of the changes of particle constitutions during the analysed sintering stages.

µ-CT of sinter materials

Two sets of samples consisting of spherical copper particles of 125...1000 µm diameter were studied (the detailed sizes and temperatures during sintering are listed in Table 1). The first set was used to test if µ-CT is a useful method for the investigation of sinter materials. The samples were sintered for 1 hour at a temperature of 1025 °C under vaccum. The µ-CT scans have been performed at the Federal Institute for Materials Research and Testing (BAM). After these first experiments two samples were prepared for the analysis of sequences of sintering stages. Spherical copper particles of 1000 µm diameter were filled into alumina crucibles (∅ 7 mm, 4 mm high). To identify the sample orientation in each tomography image the crucibles were marked by cuts of a diamond saw. The samples were filled with a diluted solution of polyvinylpyrrolidone to fix the particles in their positions. Prior to the first sintering step and after each sintering step µ-CT images were made. The heat treatments of the samples were performed in a hydrogen atmosphere. The polyvinylpyrrolidone was decomposed by heating the sample with a heating rate of 5 K/min to 250 °C. After maintaining 250 °C for 30 min the samples were heated with a heating rate of 5 K/min to 600°C. After the oxide reduction (at 600 °C, 1 hour) the samples were heated to the sintering temperature with 5 K/min. Then the copper powder was sintered for 1 hour.

Tab. 1. List of the samples

Sample ID	Measurement ID	Particle sizes [µm]	Sinter temperature [°C]
0624	0624	750	1025
0639 0638	0639 0638	750>x>500 500>x>350	1025 1025
0625	0625	350>x>125	1025
04042002.4	12042002.4.0.3	1000	Not sintered
04042002.4	17042002.4.1.1	1000	850
04042002.4	19042002.4.2.1	1000	950
04042002.4	29042002.4.3.1	1000	1000
04042002.4	06052002.4.4.1	1000	1050
11042002.5	15042002.5.0.2	1000	Not sintered
11042002.5	18042002.5.1.1	1000	950
11042002.5	10052002.5.2.1	1000	1050

Figure 1 shows a scheme of the µ-CT system used for analysis of the copper powder samples. The device consists of a microfocus X-ray tube (1), a manipulator for the sample (2) and a scintillator (3) with an adapted CCD-camera. Inside the tube an electron beam is focused on a thin tungsten target. The small focal spot emits X-ray bremsstrahlung and projects an enlarged X-ray transmission image (projection) on the scintillator. Usual settings were an acceleration voltage of 175 KV and a tube current of 20 µA. If the beam is well adjusted, the target current is 12…12.6 µA. Due to thermal expansion of the X-ray tube during the scanning process the beam adjustment changes. To reduce this effect, the X-ray tube was operated at least 1.5 hours prior to the measurements. The measurements were interrupted two times to check the target current and depending on this current a beam adjustment has been performed. In case of significant changes of the target current all images made before the beam readjustment were removed. After each exposure (usual exposure time: 550 ms) the sample was rotated by

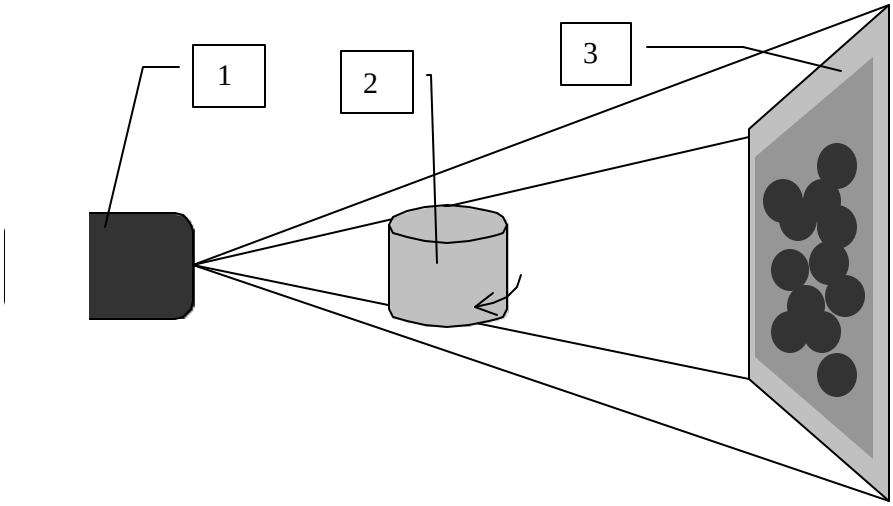

Fig. 1. Scheme of a microfocus computer tomograph

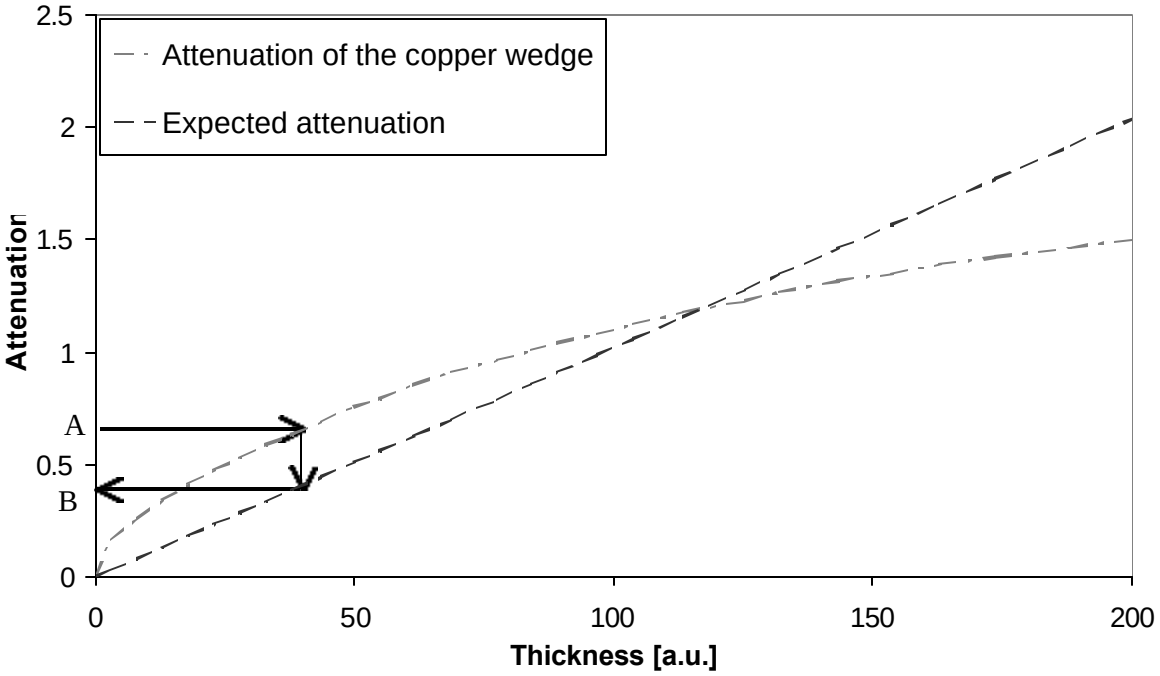

Fig. 2. Measured and expected attenuation of a copper wedge

0.5 degrees to obtain the 720 projections required for a good 3-D image quality (total time of measurement: approx. 3 hours). The detector calibration was performed by making 11 images without sample prior and after the measurement of the sample. The images of the sample were divided by the average of the calibration images.

The absorption of low energy (soft) X-ray radiation is higher than the absorption of high energy (hard) X-ray radiation. Thus the apparent absorption coefficient of any material is getting lower with growing material thickness. This effect is known as edge hardening. It can be suppressed by using a filter to shift the spectrum towards higher energies (2 mm Cu and an Al filter). Another possibility is a software algorithm based on the ideas of medical tomography [7]. The X-ray absorption of a copper wedge is measured to determine a relation between attenuation given by $-\log(I/I_0)$ where I is the intensity measured with filter and I_0 is the intensity measured without filter and the thickness of a copper layer. An example is shown

in Fig. 2. This relation is linear if no edge hardening occurs. Thus the measured attenuations of each pixel of the sample images (see: Fig. 2 point A) were replaced by the corresponding expected attenuations (see: Fig. 2 point B). By this transformation of the greyscale the edge hardening is suppressed as shown in Fig. 3.
After the greyscale transformation a distorsion correction was performed. The last step was a reconstruction of a 3-D density distribution (given as a 3-D image) by a Feldkamp algorithm.

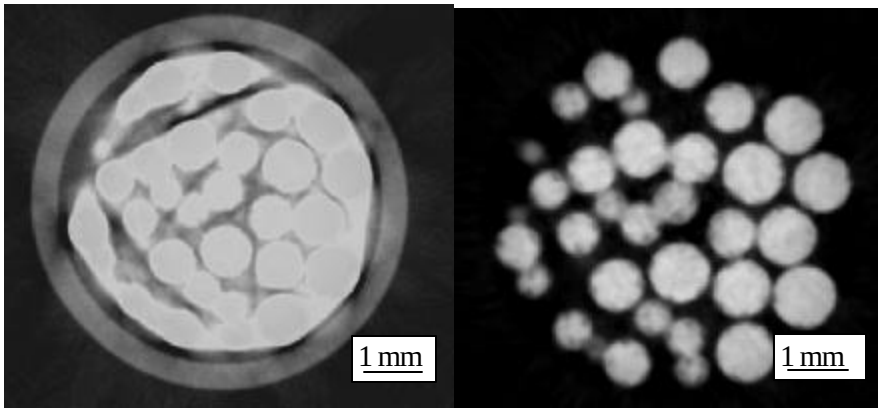

a) b)

Fig. 3. Slices of 3-D images a) without edge hardening correction b) with edge hardening correction using the described software algorithm

Sinter experiments

The characterisation of sinter models requires the description of particle positions, the distribution of distances to the next neighbours, the number of sinter necks per particle, the sinter neck geometry, the particle surface area and the particle volume. Except the number and geometry of sinter necks, these parameters were measured by image analysis. To determine the number of sinter necks by image analysis is very difficult and therefore attributed to be not very reliable. The calculation of the Euler number gives another value for the connectivity (number of sinter necks), which differs significantly from that obtained by image analysis. For the sinter neck geometry first results have been obtained, nevertheless there is need for further development.

Results

Figure 4 shows the image of the sintered sample 0625 (13.93 µm voxel size). The results of the analysis of the first samples is summarized in Table 2 (connectivity calculated using the Euler number). As the average coordination of the particles in sample 0624 is very low (assuming a krz- structure the coordination would be 4,8) this sample was analysed in detail as listed in table 3.

Tab. 2. Results of the analysis of the first samples

Measurement	Number of particles	Number of sinter necks per particle
0624	133	3.82
0625	1986	5.11
0638	1308	4.71
0639	512	5.57

Tab. 3. Results of the analysis of sample 0624

Average particle diameter	855 µm
Minimal particle diameter	35 µm
Maximal particle diameter	1400 µm
Average distance	790 µm
Average volume Minimal volume	$3.77 * 10^8$ µm^3 22800 µm^3
Maximal volume	$1.46 * 10^9$ µm^3
Total volume (by voxel counting)	$4.81 * 10^{10}$ µm^3
Average surface	$2.41 * 10^6$ µm^2
Minimal surface Maximal surface	3900 µm^2 $6.22 * 10^6$ µm^2
Total surface	$3.08 * 10^8$ µm^2

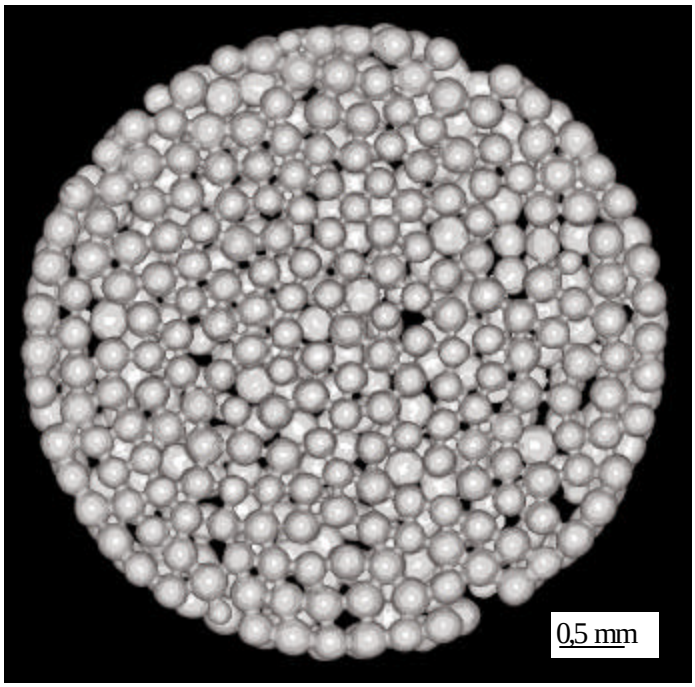

Fig. 4. 3-D image of sample 0625

Figure 5 shows X-ray transmission images of sample 04042002.4: (a) before sintering, (b) after the first sintering step at 850 °C, (c) sintered at 950 °C. Figure 5 d shows an image (the projections shown in c and d are not identical) of the sample after transformation of the greyscale. Obviously the sample was expanded after the first sintering step at 850 °C and slightly shrank as result of a second sintering step at 950 °C. This behaviour must be found in the results of the analysis of the 3-D images if the algorithms we use are correct. The applied test was an analysis of the distances between next neighbours.

The distributions of distances between next neighbour particles of sample 04042002.4 (a) and sample 11042002.5 (b) are shown in figure 6. As expected from the comparison of the images in fig. 5 the distances (measured as peak positions of the distance distributions) between next neighbour particles of sample 04042002.4 were increased from 955 µm to 970 µm after the first sintering step at 850 °C. After the second sintering step at 950 °C the peak position of the distance distribution was at 955 µm and the average distance was smaller than before sintering. As we found only 81 instead of 82 particles after the second sintering step we have

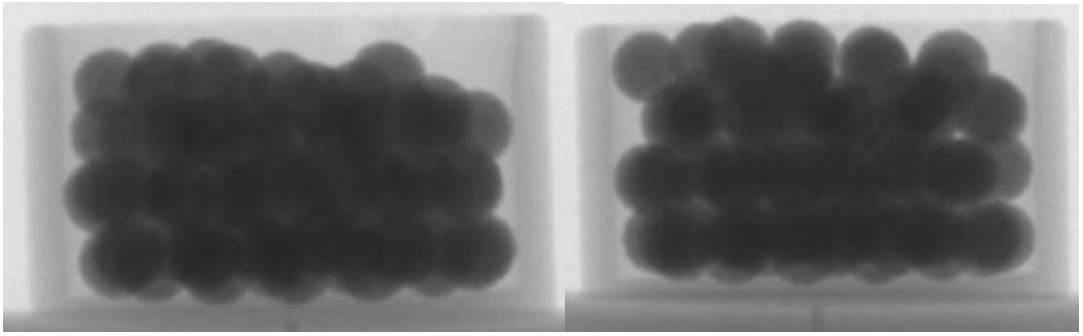

a) calibrated image, prior to sintering b) calibrated image, sintered at 850°C

c) calibrated image, sintered at 950°C d) image after edge hardening correction

Fig. 5. X-ray transmission images of sample 04042002.4

to assume, that one particle fell of the top of sample. Therefore we assume an error of 1,23% in the results of the analysis of the second sintering step. After the third sintering step at 1000 °C a further approach of the particle centres is detected (new peak of distribution: 950 µm). After the third sintering step we assume an error of about 4%. The last sintering step at 1050 °C the peak of the distance distribution was at 955 µm and the average distance was greater than after the previous sintering step. To elucidate the influence of the frequent interruptions of the sintering process on the determined results the second sample (11042002.5) was sintered at 950 °C. After sintering the peak of distance distribution of this second sample was at the same distance as prior to sintering (970 µm). As already observed in the measurements of the other sample, the distances between the particle centres after the sintering step at 1050 °C was 5 µm (new peak position: 975 µm). This single measurement cannot be used to prove that no significant error occurs due to the interruption of the sintering process, but in the future this issue will be clarified when more datasets of samples measured we will be able to distinguish between the influence of interrupted sintering, statistical variations and sample geometry.

Our main interest was the formation and breaking of contacts between particles during sintering. We assume an error of 10%[1] in the number of sinter necks determined by image analysis. The coordination histogram of sample 04042002.4 is presented in figure 7. In sample 04042002.4 the most common coordination is 5, followed by 4 and coordinations above 7 are very rare. During the first sintering step at 850°C the number of particles with coordination numbers of 6 and 7 decreased approx. 40%, proving the loss of contacts of some

[1] Our image analysis software distinguishes particle voxels from the surrounding air by setting a global density threshold. To determine the error in the number of sinter necks we performed the analysis of a 3D image several times. The first applied thresholds optimally reproduced the structure. The threshold was increased in steps of 10% until differences between the resulting structure and the original image were visible. The difference of the total number of sinter necks between the first and last analysis was about 10%.

particles. After the second sintering step the number of particles with coordination number 5 decreases by 18%. The greatest increase is found for the coordination number 6 (+ 27%) and 4 (+ 14%). Thus both the breaking and forming of sinter necks seems to be proved for two sequential sintering stages of a sample. After the third sintering step at 1000 °C the number of particles with coordination number 6 increases by 36%. The number of particles with lower coordination decrease (except particles with the coordination number 3). After the last sintering step at 1050 °C the number of particles with coordination number 6 increased by 17%. This proves an increasing connectivity during the two sintering steps at 1000 °C and 1050 °C.

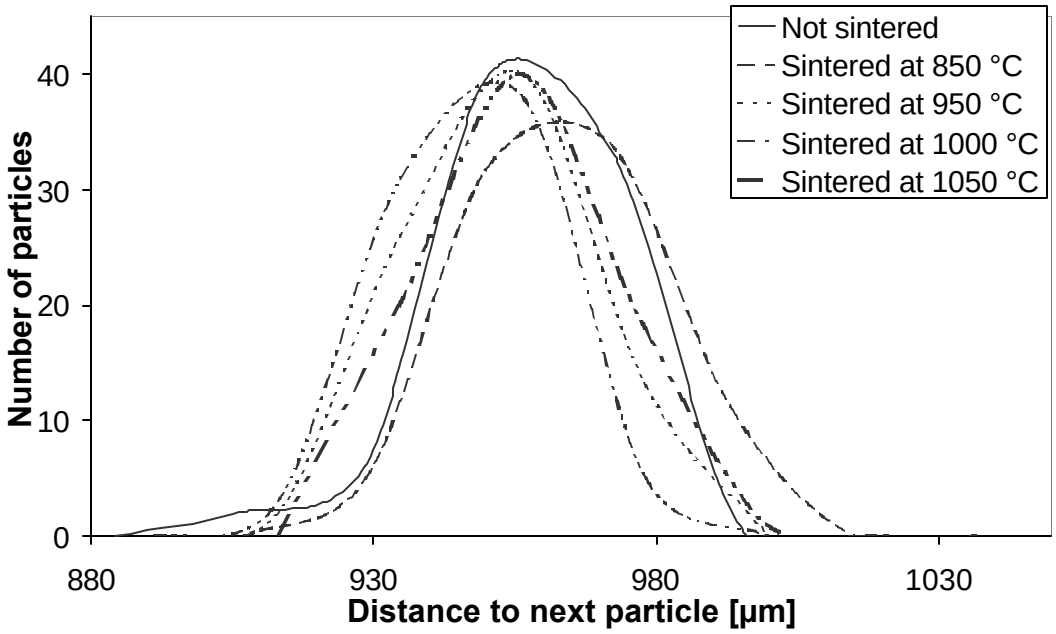

a)

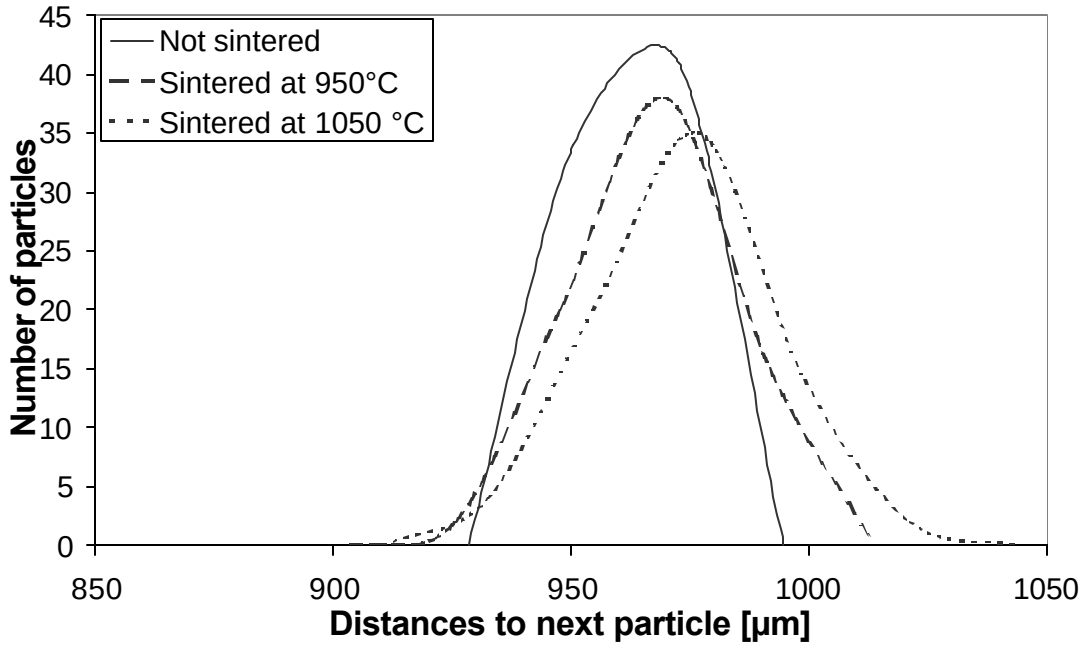

b)

Fig. 6. Distribution of distances to the next particle

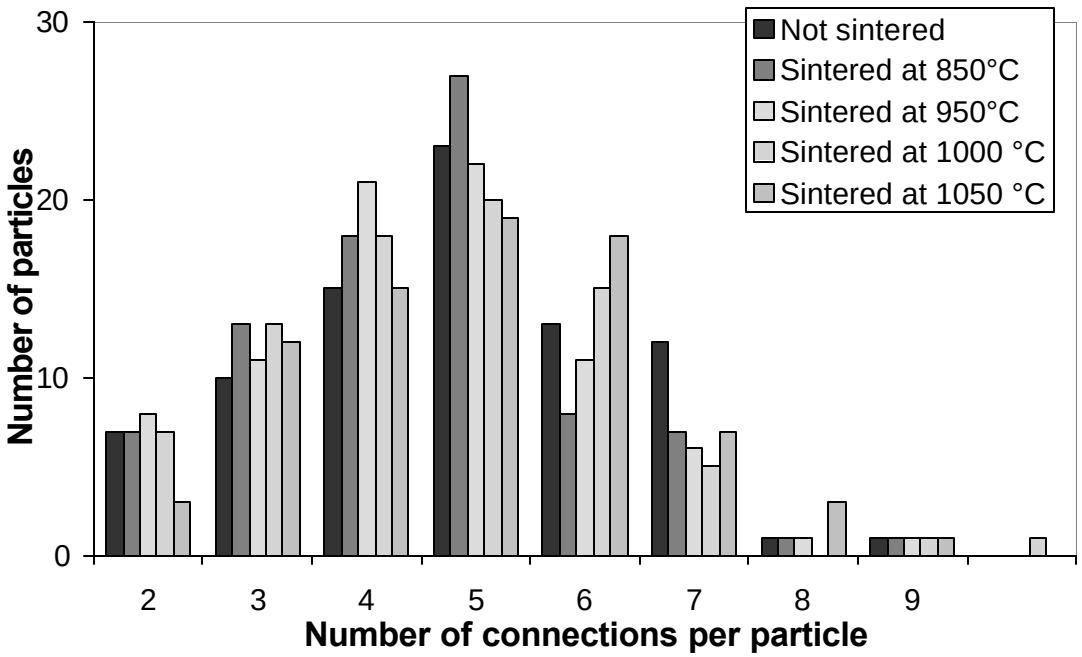

Fig. 7. Coordination histogram of sample 04042002.4

Conclusion

The use of µ-CT has been proved to be useful for the analysis of sinter processes. To be successful the samples must consist of coarse particles of at least 120 µm diameter prohibiting the application in the analysis of samples consisting of standard grade powders. The problem of edge hardening can be solved by the application of filters. This method has the disadvantage of strongly enhanced measurement times due to the decreasing total intensity. To reduce the time required for measurement a software program was developed, that allows the correction of edge hardening by measuring the attenuation of a copper wedge instead of using filters. Nevertheless due to long imaging times a real-time acquisition of data during sintering is strictly not available in the near future.
After successfully testing the method with preliminary samples the analysis of sequential sintering stages was started. The analysis of sequential sintering stages are limited to the results of image analysis. Thus the actual numbers of sinter necks of this samples probably suffer from large errors. As some changes in the coordination histogram exceed the estimated errors we are able to present the results, that seem to prove the formation and breaking of sinter necks in two sequential sintering stages. Further it could be proved, that the shrinkage and expansion of the examined samples are correlated with the distance distributions of the next particles.

Acknowledgements

The authors would like to thank Dr. Goebbels of the BAM for measuring the first samples and useful discussions. We thank our project partner Dr. Ohser for useful discussions and the analysis of the first samples. Further we thank the Deutsche Forschungsgemeinschaft (DFG) for the financial support of our research.

Literature

[1] Geguzin, J.E:; Physik des Sinterns VEB Deutscher Verlag für Grundstoffindustrie, Leipzig 1973
[2] Schatt, W.; Sintervorgänge VDI-Verlag 1992
[3] Wieters, K.P.; Korngrenzeneinfluß beim defektaktivierten Sintern; Habil.; TU Dresden 1989
[4] Exner, R.E.; Grundlagen von Sintervorgängen, Gebr. Borntraeger Berlin Stuttgart 1978
[5] Kingery, W.D., Berg, M.; J. Appl. Phys. 26 (1955) 1205
[6] Schatt, W.; P Hinz powder met. Int. 20 (1988) 6, 17
[7] Imaging sytems for medical diagnostics, ed. Erich Krestel, Berlin, Munich: Siemens-Aktiengesellschaft [Abt. Verl.] 1990, ISBN 3-8009-1564-2